Check for updates

Geophysical Research Letters

RESEARCH LETTER
10.1029/2024GL112276

Changes in Atmospheric Convection Over the Indo-Pacific Warm Pool and Coupled IOD and ENSO Patterns During the Last Glacial Maximum

Xinquan Zhou[1,2], Stéphanie Duchamp-Alphonse[2], Xiaoxu Shi[3], Franck Bassinot[4], Eva Moreno[5], Xiaobo Jin[1], Luc Beaufort[6], and Chuanlian Liu[1]

[1]State Key Laboratory of Marine Geology, Tongji University, Shanghai, China, [2]Université Paris-Saclay, CNRS, GEOPS, Orsay, France, [3]Southern Marine Science and Engineering Guangdong Laboratory (Zhuhai), Zhuhai, China, [4]Laboratoire des Sciences du Climat et de l'Environnement, CEA/CNRS/UVSQ, Université Paris-Saclay, Centre CEA-Saclay, Gif-sur-Yvette, France, [5]Laboratoire d'Océanographie et du Climat, Sorbonne Université/CNRS/IRD/MNHN, Paris, France, [6]Centre de Recherche et d'Enseignement des Géosciences de l'Environnement, CNRS/IRD, Aix-Marseille Université, Aix-en-Provence, France

Abstract This study investigates how the convection over the Indo-Pacific Warm Pool responds to the Last Glacial Maximum conditions. Paleoproductivity records that can indicate seasonal wind dynamics are combined with modeling data. Seasonal southeasterly and northeasterly winds off Sumatra are both strengthened, meanwhile, anomalous westerly winds occur over the western Celebes Sea. This reflects a zonal "tripole" pattern of the changed convection that is weakened over the exposed Sunda and Sahul shelves and strengthened over the eastern equatorial Indian Ocean and western equatorial Pacific. Model results suggest that lower sea levels and larger ice sheets are responsible for these changes. Coupled with the changed atmospheric circulation, a positive Indian Ocean Dipole-like mean state forms in the Indian Ocean. The Pacific likely exhibits an "eastern Pacific La Niña"-like superposed by a "central Pacific El-Niño"-like mean state. Under such configuration, the Indian Ocean Dipole and El Niño-Southern Oscillation variability probably strengthen.

Plain Language Summary Today, the atmospheric circulation over the Indo-Pacific Warm Pool exhibits strong convective updraft and heavy precipitation. In this study, we found evidence that the response of this atmospheric convection to Last Glacial Maximum conditions may have exhibited spatial variability, weakening in the central part associated with exposed Sunda shelf, but strengthening to the east and the west. This interpretation is proven by both, marine paleoproductivity records interpreted as indicators of seasonal surface wind intensity, and paleoclimate modeling. As the Last Glacial Maximum featured cooler temperatures and lower greenhouse gas concentrations than present, these findings provide new insight into future projections under anthropogenic increase of greenhouse gas. However, lower greenhouse gases were not the only difference during the LGM compared to today. Using numerical simulations, we evaluated the effects of individual forcing factors such as changed insolation, more extensive ice sheets, lower sea level, and lower greenhouse gases. Results suggest the expanded ice sheets and reduced sea level were primary drivers of the atmospheric convection shift over the warm pool, rather than the greenhouse gas reduction alone. Together with the change in atmospheric convection, positive-like Indian Ocean Dipole and La Niña-like conditions might occur over the Indian and Pacific Oceans, respectively.

Key Points:

- An anomalous zonal "tripole" pattern of changed Indo-Pacific Warm Pool (IPWP) convection is found during LGM
- Relatively low sea-level and large ice-sheets behind alter IPWP convection
- A positive IOD-like mean state and an "eastern Pacific La Niña"-like superposed by a "central Pacific El-Niño"-like mean state are proposed

Supporting Information:

Supporting Information may be found in the online version of this article.

Correspondence to:

X. Zhou and X. Shi,
xinquan_zhou@tongji.edu.cn;
shixiaoxu@sml-zhuhai.cn

Citation:

Zhou, X., Duchamp-Alphonse, S., Shi, X., Bassinot, F., Moreno, E., Jin, X., et al. (2025). Changes in atmospheric convection over the Indo-Pacific warm pool and coupled IOD and ENSO patterns during the last glacial maximum. *Geophysical Research Letters*, *52*, e2024GL112276. https://doi.org/10.1029/2024GL112276

Received 29 AUG 2024
Accepted 7 MAR 2025

Author Contributions:

Conceptualization: Xinquan Zhou, Stéphanie Duchamp-Alphonse, Xiaoxu Shi
Data curation: Xinquan Zhou, Xiaoxu Shi
Formal analysis: Xinquan Zhou
Funding acquisition: Xinquan Zhou, Chuanlian Liu
Investigation: Xinquan Zhou, Luc Beaufort
Methodology: Xiaoxu Shi
Resources: Stéphanie Duchamp-Alphonse, Franck Bassinot, Eva Moreno, Xiaobo Jin
Visualization: Xinquan Zhou
Writing – original draft: Xinquan Zhou

© 2025. The Author(s).
This is an open access article under the terms of the Creative Commons Attribution License, which permits use, distribution and reproduction in any medium, provided the original work is properly cited.

1. Introduction

The atmospheric convection over the Indo-Pacific Warm Pool (IPWP) results in heavy rainfall (>2,000 mm per year) over the so-called Maritime Continent (Indonesian archipeago) (De Deckker, 2016). This region forms a key component of the Walker circulation, which sustains zonal atmospheric cells over the equatorial Indian and Pacific Oceans. Interannual changes in IPWP convection are closely linked to the Indian Ocean Dipole (IOD) and El Niño-Southern Oscillation (ENSO) dynamics, and hence to anomalous zonal variations in sea surface temperatures over the equatorial Indian and Pacific Oceans (Chang et al., 2004; Hendon, 2003; Hendrawan et al., 2019; Saji & Yamagata, 2003; Supari et al., 2018; Yin et al., 2020). It has been shown that anomalous states of these coupled atmosphere-ocean systems can have far-reaching impacts. For instance, a reduction in IPWP convection, coupled with positive IOD modes and/or La Niña events, can lead to extreme rainfall events with devastating consequences as far as Eastern Africa and Western America (Conway et al., 2007; Marchant

Writing – review & editing: Xinquan Zhou, Stéphanie Duchamp-Alphonse, Xiaoxu Shi, Franck Bassinot, Eva Moreno, Xiaobo Jin, Chuanlian Liu

et al., 2006; Ropelewski & Halpert, 1986; Tedeschi et al., 2013). Given the role of IPWP convection in shaping tropical climates, it is imperative to deepen our understanding of its dynamics in conjunction with IOD and ENSO patterns, particularly in the context of ongoing global warming. As future projections heavily depend on earth system models, it is also important to evaluate models' ability to accurately replicate climate features and sensitivities to changed boundary conditions. The Last Glacial Maximum (LGM; 23−19 ka), characterized by more extensive ice sheets, lower sea level, and reduced greenhouse gases compared to preindustrial times, serves as a key benchmark within the Paleoclimate Modeling Intercomparison Project (PMIP; Braconnot et al., 2012; Kageyama et al., 2018). The transition from the LGM to the Holocene represents a natural warming phase, and the climatic effects of this transition can be reconstructed using paleoclimatic data together with numerical simulations.

Many studies have previously focused on hydroclimate conditions in regions influenced by the Walker circulation to reconstruct past changes in IPWP convection (e.g., Carolin et al., 2013; DiNezio et al., 2018; DiNezio & Tierney, 2013; Niedermeyer et al., 2014; Partin et al., 2007; Ruan et al., 2019; Wurtzel et al., 2018; Yu et al., 2023). While proxy records provide valuable local to regional insights into climate changes, numerical simulations can depict large-scale atmospheric circulation patterns, and proxy-model comparisons have been widely used in this region to better interpret paleoclimate changes (Chevalier et al., 2017; DiNezio et al., 2018; DiNezio & Tierney, 2013; Mohtadi et al., 2017; Zhou et al., 2023). However, significant discrepancies persist among studies, particularly when dealing with the LGM (e.g., Brierley et al., 2023; DiNezio & Tierney, 2013; Mohtadi et al., 2017). On the one hand, based on hydroclimate proxies and outputs from the HadCM3 and CESM1.2 models, DiNezio and Tierney (2013) and DiNezio et al. (2018) have suggested a weakened IPWP convection, accompanied by a reduced Indian Ocean Walker circulation and a positive IOD-like mean state. On the other hand, Mohtadi et al. (2017) have argued for an intensification of the Indian Ocean Walker circulation, with a negative IOD-like mean state, according to paleo-thermocline records from the eastern equatorial Indian Ocean (EEIO) and results of the CCSM3 and FGOALS-g1.0 models. In the Pacific, Koutavas and Joanides (2012) and Dang, Jian, et al. (2020) have documented an El Niño-like mean state, based on sea surface temperature (SST) reconstructions from the western (WEP) and eastern equatorial Pacific (EEP). In contrast, a more recent study focusing on SST records has argued for La Niña-like mean states during glacial periods (Zhang et al., 2023). None of these studies took into account SST changes in the central equatorial Pacific (CEP), despite their key role in defining El Niño/La Niña conditions. Monteagudo et al. (2021) have highlighted this gap, reporting weaker cooling in the CEP compared to the WEP and EEP, and suggesting non-monotonic anomalous SST gradient aross the equatorial Pacific. Moreover, there is limited consensus among PMIP modeling results regarding changes in the SST zonal gradient and the Walker circulation over the Pacific (Brown et al., 2020; DiNezio et al., 2011; Tian & Juang, 2019). Beyond the hydroclimate and SST reconstructions, relatively few studies have aimed at directly reconstruct atmospheric dynamics (Bassinot et al., 2011; Mohtadi et al., 2017; Zhou et al., 2024).

Atmospheric dynamics can be inferred from preserved evidence of the impact that surface winds exert on upper seawater properties. In specific environments, such as coastal upwelling systems, stronger winds shoal the thermocline and the nutricline, enhance the delivery of nutrients from intermediate/deep layers into the sunlit near-surface, and increase the net primary productivity (NPP) (McCreary et al., 2009). Weaker winds have the reverse effect. Consequently, variations in past wind intensity can be deduced from reconstructed NPP (e.g., Lückge et al., 2009; Zhou et al., 2024). In tropical oceans, the abundance of the deep-dwelling coccolithophore *Florisphaera profunda* is directly linked to the nutricline dynamics (Molfino & McIntyre, 1990), and serves as a powerful proxy for reconstructing NPP (Beaufort et al., 1997; Hernández-Almeida et al., 2019). It is suggested to be insensitive to SST changes but highly responsive to wind-driven processes, such as mixing and upwelling (Hernández-Almeida et al., 2019), and has proven to be particularly effective in the equatorial Indian Ocean and the IPWP region (e.g., Zhou et al., 2023, 2024).

This study aims to investigate how IPWP convection may have been modified under LGM conditions and its linkage to the altered IOD and ENSO patterns. Changes in IPWP convection are reconstructed through seasonal wind dynamics inferred from NPP records. Two NPP reconstructions from coastal upwelling regions off Sumatra, influenced by the IOD, are expected to capture seasonal wind patterns (Figure 1). Indeed, summer-autumn southeasterly winds off southern Sumatra and winter northeasterly winds off northern Sumatra are known to specifically pull out deep-layer waters to the surface and increase NPP. Modern observations and modeling indicate that NPP in these regions anomalously increases under positive IOD events, when the seasonal winds driving upwelling strengthen (Currie et al., 2013; Lévy et al., 2007; Wiggert et al., 2009; Figure 1). One NPP

19448007, 2025, 6, Downloaded from https://agupubs.onlinelibrary.wiley.com/doi/10.1029/2024GL112276 by Ifremer Centre Bretagne Blp, Wiley Online Library on [21/03/2025]. See the Terms and Conditions (https://onlinelibrary.wiley.com/terms-and-conditions) on Wiley Online Library for rules of use; OA articles are governed by the applicable Creative Commons License

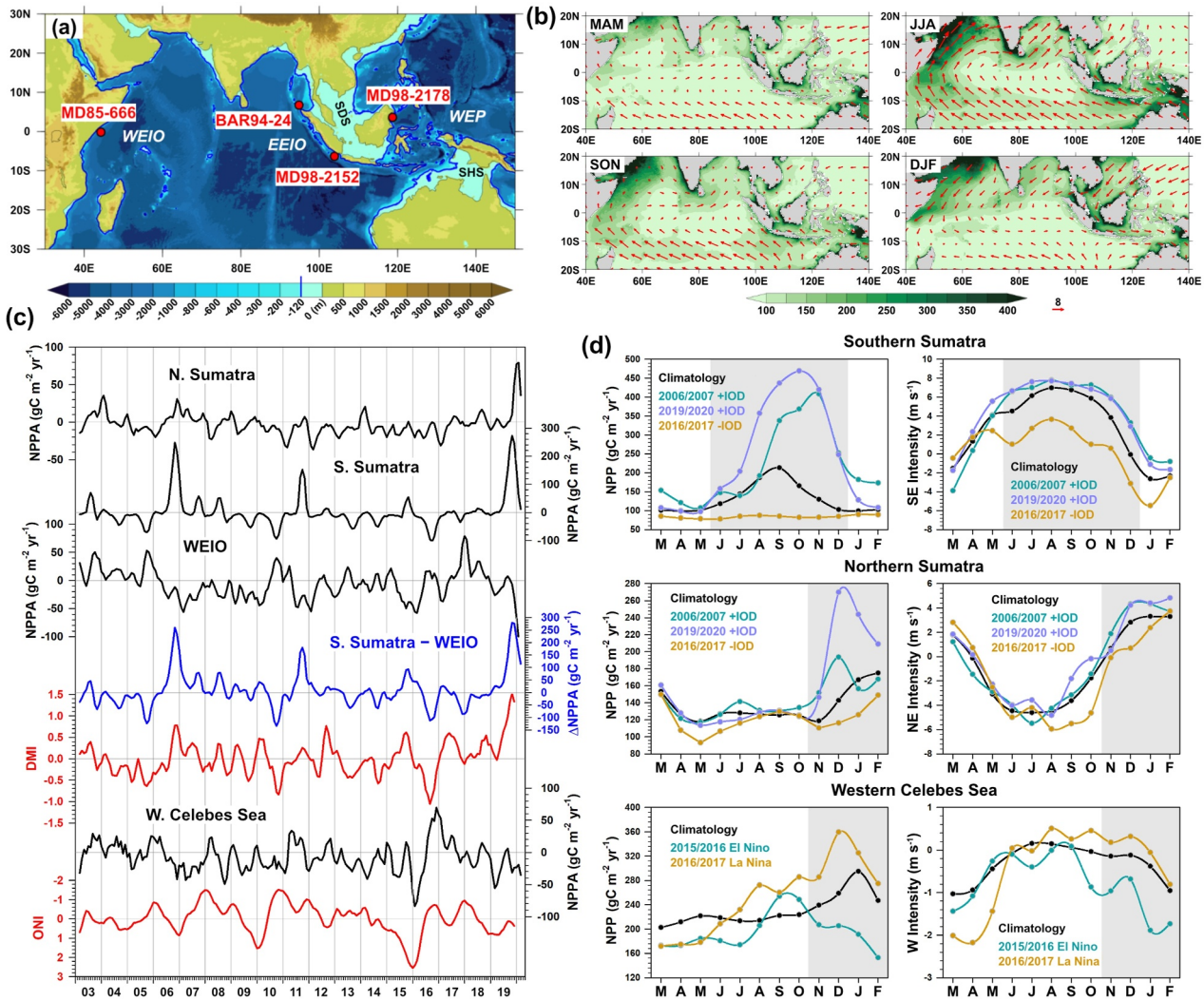

Figure 1. (a) Geography setting and bathymetry (GMRT4.2; Ryan et al., 2009) of the study area. Locations of sites for net primary productivity (NPP) reconstructions are marked by red dots. The blue contour lines highlight the −120 m level, which approximately corresponds to the coastlines during the LGM. The abbreviations are as follow: WEIO = Western equatorial Indian Ocean; EEIO = Eastern equatorial Indian Ocean; WEP = Western equatorial Pacific; SDS = Sunda shelf; SHS = Sahul shelf. (b) Seasonal mean (years 2003–2020) NPP (gC m^{-2} yr^{-1}) and surface wind (m s^{-1}). (c) 3-point moving averages of monthly NPP anomaly (gC m^{-2} yr^{-1}) from years 2003 to 2020 in four regions in the equatorial Indian Ocean, that is, offshore northern Sumatra (5°N−7°N, 91°E−98°E), offshore southern Sumatra (5°S−10°S, 101°E−106°E), in the western western equatorial Indian Ocean (3°N−3°S, 42°E−48°E), and the western Celebes Sea (2°N−4°N, 118°E−119°E); Difference of NPP anomaly between southern Sumatra and WEIO; The Dipole Mode Index (DMI; Saji et al., 1999) and Ocean Niño index (ONI; https://svs.gsfc.nasa.gov/30847/). (d) Seasonal cycles of NPP, northeasterly (NE), southeasterly (SE), and westerly (W) winds over aforementioned regions of climatological (years 2003–2020) and Indian Ocean Dipole/El Niño-Southern Oscillation years. The gray bars mark the upwelling seasons. NPP was calculated by the standard VGPM model based on the MODIS chlorophyll-a concentration data (Behrenfeld & Falkowski, 1997). NPP data are from the "Ocean Productivity" website (http://sites.science.oregonstate.edu/ocean.productivity). Wind data are from the ERA5 reanalysis data sets (Hersbach et al., 2020).

reconstruction from the western equatorial Indian Ocean (WEIO) is compared to the eastern records to examine potential zonal gradients associated with IOD-like mean states (Figure 1). At last, one NPP record from the western Celebes Sea, close to the equator and influenced by ENSO, is expected to be sensitive to changes in the zonal wind pattern (Figure 1). It appears indeed, La Niña conditions associated with stronger westerly winds, increase NPP in this region (Figure 1; Zhou et al., 2023). In complement, SST reconstructions from the equatorial Indian and Pacific Oceans are revisited, and together with the 4 aforementioned NPP, they are compared to atmospheric and oceanic outputs from LGM experiments conducted using 6 PMIP4 models (Kageyama et al., 2017), to evaluate changes in IPWP convection, as well as IOD and ENSO patterns. Sensitivity experiments run with AWI-ESM-1-1-LR (termed AWI-ESM in the following) also help isolating the individual effects of

19448007, 2025, 6, Downloaded from https://agupubs.onlinelibrary.wiley.com/doi/10.1029/2024GL112276 by Ifremer Centre Bretagne Blp, Wiley Online Library on [21/03/2025]. See the Terms and Conditions (https://onlinelibrary.wiley.com/terms-and-conditions) on Wiley Online Library for rules of use; OA articles are governed by the applicable Creative Commons License

altered orbital parameters, expanded ice sheets, lower sea levels, and reduced greenhouse gas concentrations, respectively (Shi et al., 2023).

2. Materials and Methods

2.1. Reconstruction of Net Primary Productivity

NPP is reconstructed based on the relative abundance of the coccolith specie *F. profunda* (Fp%) for 4 well dated sediment cores from equatorial oceanic regions influenced by seasonal winds and IOD/ENSO events (Figure 1; Text S1, Table S1, and Figure S1 in Supporting Information S1), according to the empirical equations obtained by Hernández-Almeida et al. (2019). For cores BAR94-24, MD98-2152, and MD85-666 collected in the tropical Indian Ocean, the following equation is used:

$$\mathrm{NPP} = \left[10^{(3.27-0.01\times \mathrm{Fp\%})}\right] \times 365/1000.$$

For core MD98-2178 collected in the western Pacific, the following one is used:

$$\mathrm{NPP} = \left[10^{(2.78-0.005\times \mathrm{Fp\%})}\right] \times 365/1000.$$

The unit of NPP is grams of carbon per meter square per year (gC m^{-2} yr^{-1}). Fp% is calculated as follow: Fp % = 100 × (Fp number/total coccolith number). The errors (1σ) of Fp% calculated following the method of Patterson and Fishbein (1989) have an average of ±2%.

2.2. Sea Surface Temperature Records

It has been shown that the Mg/Ca ratio of foraminifer shells reflects their growth temperature (Anand et al., 2003; Cléroux et al., 2008; Elderfield & Ganssen, 2000; Lea, Elderfield, & Wilson, 2000; Lea, Pak, & Spero, 2000). We compile Mg/Ca data from planktonic foraminifera *Globigerinoides ruber* in the equatorial (10°N−10°S) regions obtained by previous studies, to evaluate regional differences in the LGM cooling (Text S2, Table S2 and Figure S2 in Supporting Information S1). Following Anand et al. (2003), the Mg/Ca values are converted into SST by

$$\mathrm{Mg/Ca} = 0.038 \times e^{0.09\times \mathrm{SST}},$$

where Mg/Ca is in mmol mol^{-1} and SST is in °C. We only consider the records that continuously cover the period from LGM to late-Holocene to get regional averaged SST changes by stacking the records (Dang, Jian, et al., 2020). However, as no continuous record is available in the CEP, polynomial fitting is used to get the mean variation trends. It is noteworthy that the SST of polynomial fitting at 0 ka over the equatorial regions are comparable to observed values (Text S2 and Figure S2 in Supporting Information S1).

2.3. Paleoclimate Models and Simulations

We leverage preindustrial (PI) and LGM experiments that are in the framework of the CMIP6 and PMIP4 projects. Available outputs of 6 model running LGM experiment are analyzed (Table S3 in Supporting Information S1). Set-ups of boundary conditions in these experiments can be found in Eyring et al. (2016) and Kageyama et al. (2017). To explore the effects of single forcing factors during the LGM, we rely on results of sensitivity experiments performed with AWI-ESM, following the PMIP4 protocol (Kageyama et al., 2017; Shi et al., 2023): (a) the LGM_G, in which all boundary conditions are set to the LGM except for the greenhouse gases that are the same as for PI; (b) the LGM_I, in which all boundary conditions are set to LGM except the ice sheets that are the same as for PI; (c) the LGM_O, in which all boundary conditions are set to LGM, except the orbital parameters that are the same as for PI; (d) the LGM_GI, in which all boundary conditions are set to LGM except the greenhouse gases and ice sheets that are the same as for PI. With these sensitivity experiments, we can get the changes due to single forcing:

$$\delta\mathrm{ORB} = \mathrm{LGM} - \mathrm{LGM\_O}\ (\text{Due to altered orbital parameters})$$

$$\delta\mathrm{GAS} = \mathrm{LGM} - \mathrm{LGM\_G}\ (\text{Due to lower greenhouse gases})$$

19448007, 2025, 6, Downloaded from https://agupubs.onlinelibrary.wiley.com/doi/10.1029/2024GL112276 by Ifremer Centre Bretagne Blp, Wiley Online Library on [21/03/2025]. See the Terms and Conditions (https://onlinelibrary.wiley.com/terms-and-conditions) on Wiley Online Library for rules of use; OA articles are governed by the applicable Creative Commons License

19448007, 2025, 6, Downloaded from https://agupubs.onlinelibrary.wiley.com/doi/10.1029/2024GL112276 by Ifremer Centre Bretagne Blp, Wiley Online Library on [21/03/2025]. See the Terms and Conditions (https://onlinelibrary.wiley.com/terms-and-conditions) on Wiley Online Library for rules of use; OA articles are governed by the applicable Creative Commons License

$$\delta\text{ICE} = \text{LGM} - \text{LGM\_I (Due to larger ice sheets)}$$

$$\delta\text{GAS\_ICE} = \text{LGM} - \text{LGM\_GI (Due to lower greenhouse gases and larger ice sheets).}$$

The residual change, excluding the effects of altered orbital parameters, lower greenhou gases, and larger ice sheets, is calculated as:

$$\delta\text{RES} = (\text{LGM} - \text{PI}) - (\delta\text{ORB} + \delta\text{GAS\_ICE}).$$

The northeasterly (NE) and southeasterly (SE) wind intensities off northeastern and southeastern Sumatra respectively, are calculated for comparisons with reconstructed surface winds based on NPP records from cores BAR94-24 and MD98-2152 as follow:

$$\text{NE} = [-1 \times \text{U} \times \cos(45°)] + [-1 \times \text{V} \times \cos(45°)];$$

$$\text{SE} = [-1 \times \text{U} \times \cos(45°)] + [\text{V} \times \cos(45°)],$$

where U and V are the zonal and meridional wind speeds.

3. Results and Discussion

3.1. The Changed IPWP Convection and Glacial Forcing

Reconstructed NPP are 27% and 16% higher (student's *t*-test [$p < 0.01$]) at MD98-2152 and BAR94-24 during the LGM compared to the late-Holocene (Figure 2). These increases can be directly interpreted as evidence of strengthened summer-autumn southeasterly and winter northeasterly winds off southern and northern Sumatra, which is in agreement with Huang et al. (2024) that have recently documented increased precipitation seasonality over Sumatra and Java. Similarly, the 17% higher NPP during the LGM (student's *t*-test's [$p < 0.01$]) recorded by MD98-2178 indicates a strengthened westerly wind component (or weakened easterly wind component) over the western Celebes Sea in autumn-winter (Figure 2). Overall, the magnitude of these NPP increases during the LGM is comparable to that observed during modern positive IOD and La Niña years. Only at site MD98-2152 the NPP increase is lower. This is probably because of the influence of oligotrophic specimens in the coccolith assemblages, as this core has been retrieved in a more open oceanic environment.

Among the 6 PMIP4 models, only AWI-ESM concurrently simulates all the strengthened seasonal winds deduced from the aforementioned NPP records (Figure 3a). These simulated winds are associated with enhanced seasonal upwelling (Figure S3 in Supporting Information S1), indicating well proxy-model agreement and testifying for the superior performance of this model (Figure 3). CESM2-FV2 and CESM2-WACCM-FV2 simulate strengthened southeasterly and westerly winds but they do not reproduce strengthened northeasterlies (Figure 3a). Conversely, INM-CM4-8 simulates strengthened northeasterly and westerly winds but not southeasterlies (Figure 3a). Results of AWI-ESM are absent in MPI-ESM1-2-LR, although both models sharing the same components except for the oceanic one. A key distinguishing feature of AWI-ESM is its high-resolution unstructured oceanic meshes (Shi, Lohmann, et al., 2020; Sidorenko et al., 2015). One possible reason for the differences between AWI-ESM and MPI-ESM lies in the oceanic component used in the coupled model. The unstructured oceanic meshes in AWI-ESM may be particularly advantageous for simulating near-coastal processes and dynamics in regions with narrow straits, such as the Maritime Continent.

In AWI-ESM, the strengthened southeasterly and northeasterly winds off Sumatra are driven by anomalous high sea level pressure (SLP) during summer-winter over the northeastern and southeastern Indian Ocean, respectively (Figure S4 in Supporting Information S1). Strengthened westerly winds over western Celebes Sea are caused by the anomalous SLP gradient during autumn and winter between Maritime Continent and the western Pacific (Figure S4 in Supporting Information S1). Altogether, these configurations result in annual mean easterly winds over the EEIO and westerly winds over the WEP (Figure 3c). Accompanying the changes in surface winds, the vertical atmospheric movement over the IPWP exhibits a pattern with spatially differentiated changes: the convection is reduced over the Sunda and Sahul shelves and enhanced over the EEIO and WEP (Figures 3b and 3c). As such, the changes in IPWP convection displays a "tripole" pattern in the equatorial region, which is tightly

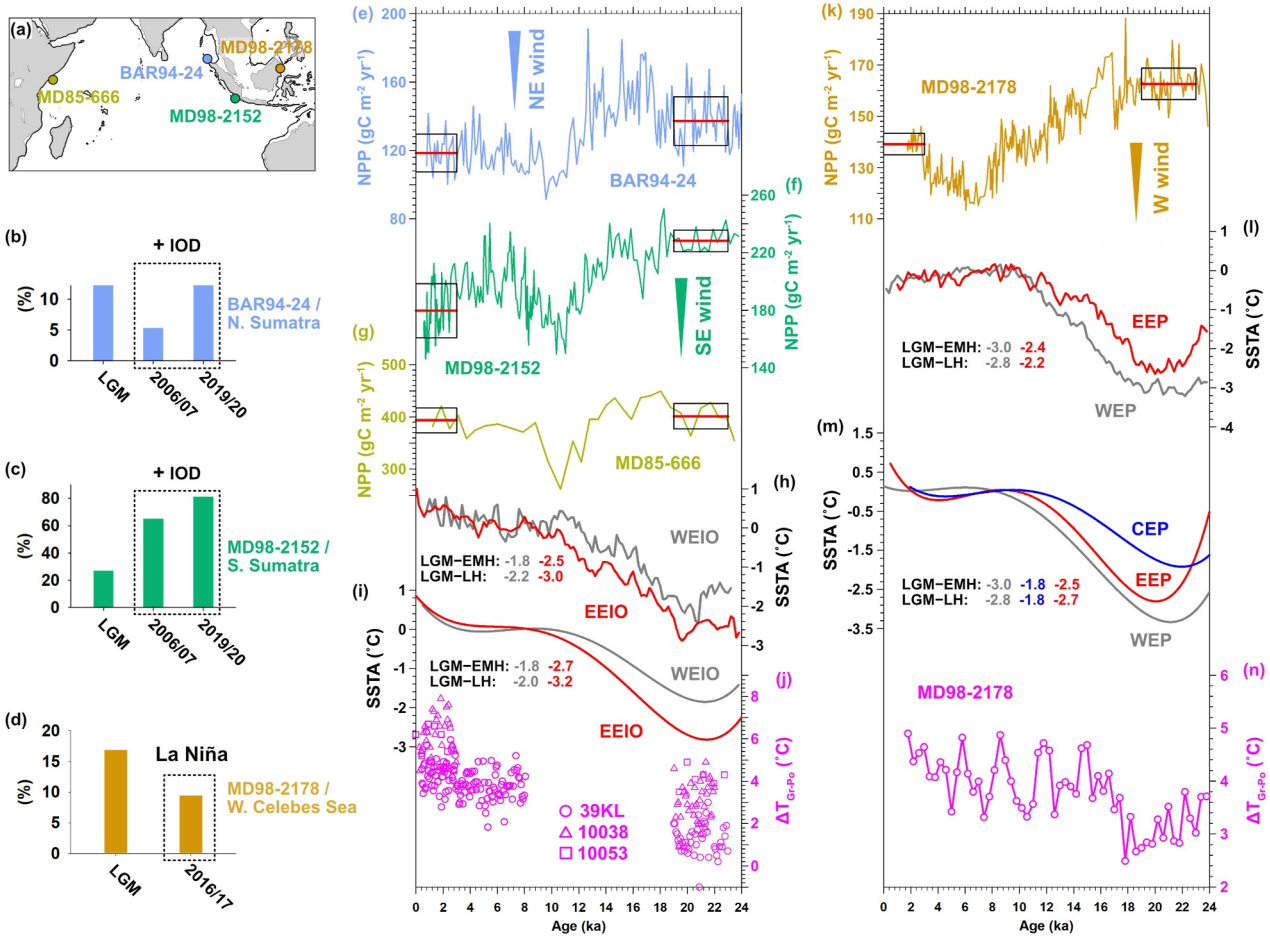

Figure 2. (a, e, f, g, k) Site locations and reconstructed net primary productivity (NPP) of the 4 studied cores. The black lines on (a) indicate the LGM coastlines. The Holocene data of MD98-2152 and MD98-2178 have been shown in Zhou et al., 2023, 2024. The red and black lines on mark the averages and 1σ of the LGM (23−19 ka) and late-Holocene (3−0 ka) values. The bar charts of (b, c, d) mark the percentage of increase in annual mean NPP, concerning the differences between LGM and late-Holocene, and between positive Indian Ocean Dipole/La Niña years and climatological mean (Figure 1). (h) The sea surface temperature (SST) anomaly stacks of western equatorial Indian Ocean (WEIO) and eastern equatorial Indian Ocean (EEIO) records. (i) The polynomial fits of WEIO and EEIO SST records. (j) Difference of temperature between estimations of *G. ruber* and *P. obliquiloculata* Mg/Ca ratios in the eastern Indian Ocean (Mohtadi et al., 2017). (i, m) As (h, i) but for Pacific records. (n) As (j) but for the western Pacific (Fan et al., 2018).

linked to two anomalous zonal circulation cells located over the EEIO and WEP, respectively (Shi et al., 2023; Figures 3b and 3c). This tripole pattern is a unique result produced by AWI-ESM, distinguishing it from other models (Figure S5 in Supporting Information S1). It also differs from the "dipole" one under the mid-Holocene conditions, which is characterized by reduced convection over the WEP and enhanced convection over the EEIO, and driven by altered tropical insolation (Zhou et al., 2023). The dipole pattern results in anomalous "trans-ocean" easterly winds blowing from the WEP to EEIO, which can drive reversed changes in NPP at sites MD98-2152 and MD98-2178 over the Holocene (Figures 2f and 2k).

Sensitivity experiments conducted with AWI-ESM indicate that the changed IPWP convection and the anomalous zonal winds over the EEIO and WEP are primarily driven by the presence of larger ice sheets and residual changes (Figure 3c), while the effects of altered orbital parameters and lower greenhouse gases are of minor importance (Figure S6 in Supporting Information S1). Beyond the forcing of ice sheets, greenhouse gases and orbital parameters, the only significant difference between the LGM and PI experiments lies in the land-sea mask associated with the glacial drop in sea level (Kageyama et al., 2017; Shi et al., 2023). Therefore, the residual changes can be primarily attributed to the lower sea level and to the associated land exposure. Specifically, larger ice sheets generate anomalous westerly winds during autumn-winter over the WEP, that contribute to the formation of the eastern zonal circulation cell. In contrast, the lower sea level causes anomalous easterly winds from

19448007, 2025, 6, Downloaded from https://agupubs.onlinelibrary.wiley.com/doi/10.1029/2024GL112276 by Ifremer Centre Bretagne Blp, Wiley Online Library on [21/03/2025]. See the Terms and Conditions (https://onlinelibrary.wiley.com/terms-and-conditions) on Wiley Online Library for rules of use; OA articles are governed by the applicable Creative Commons License

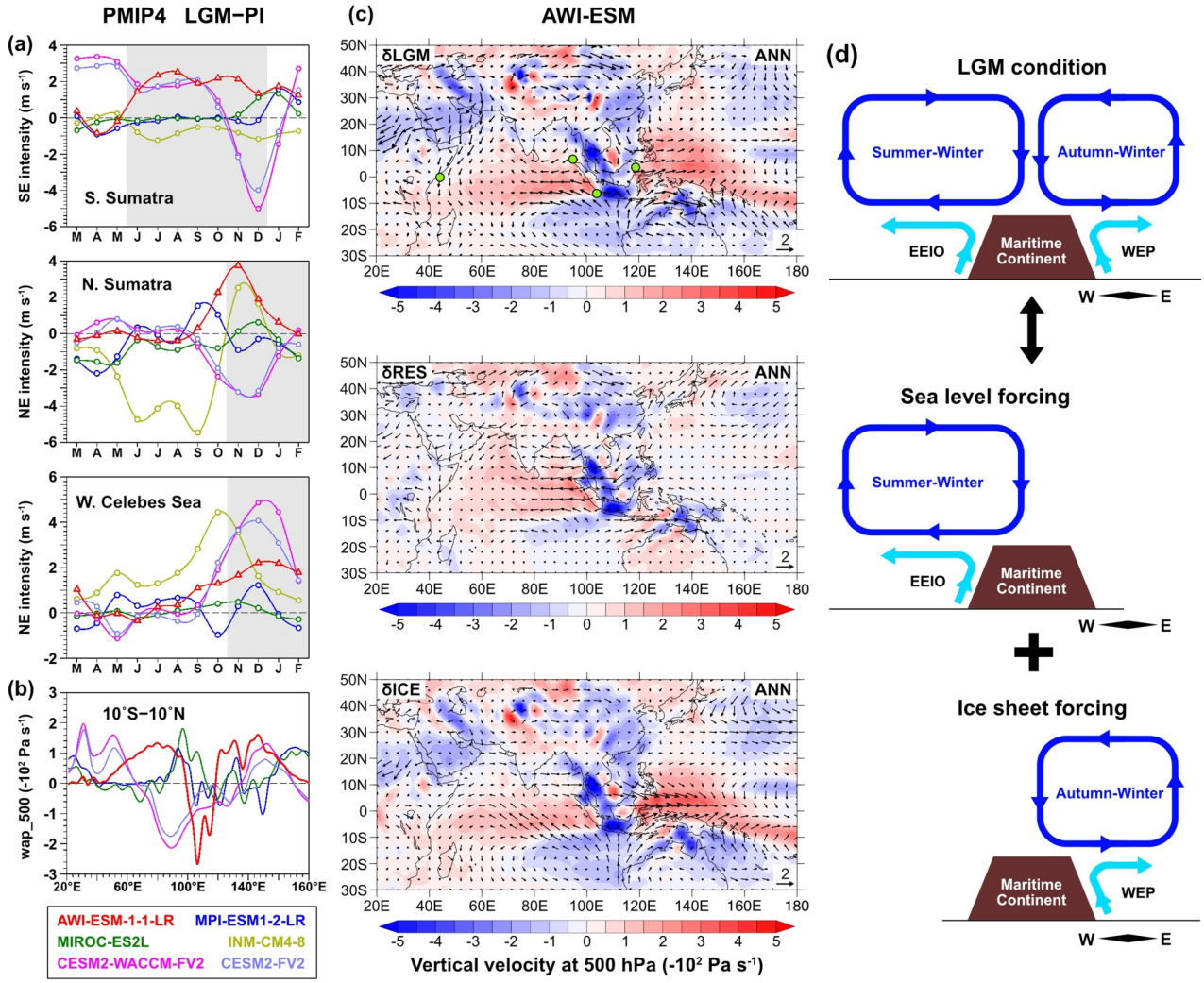

Figure 3. Results of PMIP4 and AWI-ESM modeling. (a) Simulated differences in seasonal winds between LGM and PI over northern and southern Sumatra and western Celebes Sea. The gray bars mark the upwelling seasons. (b) Simulate differences in annual mean vertical velocity at 500 hPa level between LGM and PI averaged over the equatorial region (10°S−10°N). (c) Annual mean vertical velocity at the 500 hPa atmospheric level (-10^2 Pa s^{-1}) and surface wind (m s^{-1}) simulated by AWI-ESM sensitivity experiments (δRES and δICE). The green dots mark the sites of net primary productivity reconstruction. (d) Schematic diagram of the change in atmospheric circulation over the Indo-Pacific Warm Pool related to LGM forcing.

summer to winter over the EEIO, that promote the western zonal circulation cell (Figure 3; Figure S4 in Supporting Information S1). Glacial sea level changes are thought to have a substantial impact on the IPWP climate (Dang, Wu, et al., 2020; DiNezio & Tierney, 2013; Wu et al., 2013). Particularly, Di Nezio et al. (2016) have emphasized the role of exposed Sunda and Sahul shelves, akin to the enhanced Bjerknes feedback, on driving the anomalous cooling and (south-) easterly winds in the (south-) eastern Indian Ocean. Their findings, based on sensitivity experiments run with CESM1.2, are consistent with those of AWI-ESM, which also show anomalous high SLP over the Maritime Continent and eastern Indian Ocean from summer to winter (residual changes in Figure 3; Figure S4 in Supporting Information S1).

For the Indian Ocean, it appears that CESM1.2, CESM2-FV2 and CESM2-WACCM-FV2 simulate anomalous easterly winds off Sumatra extending to the WEIO (Di Nezio et al., 2016, 2018; Figure 3a), whereas AWI-ESM confines these winds to the EEIO. Additionally, the CESM models simulates anomalous southeasterly winds, rather than northeasterly winds, in contrast to the northeasterly winds simulated by AWI-ESM. Notably, AWI-ESM sensitivity experiments highlight the role of expanded ice sheets in modifying IPWP convection. The anomalous westerly winds over the WEP are likely linked to anomalous warming (or reduced cooling) in the tropical Pacific under the larger ice sheets (Figure S6 in Supporting Information S1). This warming results in

19448007, 2025, 6, Downloaded from https://agupubs.onlinelibrary.wiley.com/doi/10.1029/2024GL112276 by Ifremer Centre Bretagne Blp, Wiley Online Library on [21/03/2025]. See the Terms and Conditions (https://onlinelibrary.wiley.com/terms-and-conditions) on Wiley Online Library for rules of use; OA articles are governed by the applicable Creative Commons License

19448007, 2025, 6, Downloaded from https://agupubs.onlinelibrary.wiley.com/doi/10.1029/2024GL112276 by Ifremer Centre Bretagne Blp, Wiley Online Library on [21/03/2025]. See the Terms and Conditions (https://onlinelibrary.wiley.com/terms-and-conditions) on Wiley Online Library for rules of use; OA articles are governed by the applicable Creative Commons License

anomalous low SLP over the WEP and CEP, causing westward-blowing winds from the Maritime Continent to the equatorial Pacific (Figure S6 in Supporting Information S1).

Additionally, decreasing trends in NPP over the deglacial period (16–11.5 ka) are observed at the 3 aforementioned sites located within the IPWP (Figure 2). These trends reflect the waning of LGM conditions, including a rising sea level and a shrinking ice volume. As these changes occur, the anomalous tripole pattern of IPWP convection weakens and naturally leads to a reduction in the anomalous easterly winds over the EEIO and westerly winds over the WEP.

3.2. A Positive IOD-Like Mean State

The anomalous easterly winds over the EEIO testify for a weakened Indian Ocean Walker circulation, potentially linked to a positive IOD-like mean state. This assumption is supported by the NPP data from site MD85-666. As this site located in a productive region of the WEIO that is, outside the IPWP (Figure 1), reconstructed NPP is generally higher than in the EEIO (Figure 2), but shows little change between the LGM and late-Holocene (student's *t*-test [$p = 0.3$]). In contrast, NPP significantly increases in the EEIO during the LGM (Figure 2).

The positive IOD-like mean state is further supported by previously published SST data, which show stronger cooling in the EEIO compared to the WEIO (Figure 2). The anomalous negative east-west SST gradient over the Indian Ocean is also simulated by AWI-ESM (Figure S3 in Supporting Information S1). Moreover, larger standard deviation in summer and autumn SST in the EEIO and WEIO suggest stronger IOD variability during the LGM (Figure S3 in Supporting Information S1). This aligns with previous studies based on individual foraminifera oxygen isotope measurements showing larger variability during the LGM (Abram et al., 2020; Thirumalai et al., 2019).

Mohtadi et al. (2017) have reconstructed mixed-layer and thermocline temperatures in the region off Sumatra, based on *G. ruber* and *Pulleniatina obliquiloculata* Mg/Ca signals respectively, and have used their differences (ΔT_{Gr-Po}) to infer variations in thermocline depth. They have found that ΔT_{Gr-Po} in the EEIO is smaller during the LGM compared to the late-Holocene, indicating a deeper thermocline and hence, a negative IOD-like mean state (Interpretation A in Figure S7 in Supporting Information S1). However, this interpretation assumes for a fixed *P. obliquiloculata*'s calcification depth (~75 m) over time, which may not be valid. More recently, Dang et al. (2018) show that the calcification depth of *P. obliquiloculata* in upwelling systems is likely controlled by seawater vertical movements, with the depth becoming shallower during upwelling seasons, thereby approaching to the calcification depth of *G. ruber* (Text S3 and Figure S7 in Supporting Information S1). In this context, the smaller ΔT_{Gr-Po} during the LGM could be interpreted as a result of the closer calcification depths of the two foraminifera species due to enhanced coastal upwelling intensity (Interpretation B in Figure S6 in Supporting Information S1). Furthermore, if more frequent positive IOD events occur during LGM, it is plausible that *P. obliquiloculata* with calcification depths closer to those of *G. ruber* are more commonly produced during upwelling seasons, thus resulting in the smaller ΔT_{Gr-Po} (Figure 2j). Similarly, this mechanism could also apply to the western Celebes Sea, where a lower LGM ΔT_{Gr-Po}, coinciding with higher NPP, might indicate a shallower thermocline depth (Figure 2n).

3.3. A La Niña-Like Mean State

In modern observations, NPP in the western Celebes Sea increases under La Niña conditions (Figure 1). Accordingly, a La Niña-like mean state can be inferred from the increased NPP during the LGM observed in MD98-2178 (Figure 2), which is in apparent contradiction with previous studies that have suggested an El Niño-like mean state over the Pacific. Indeed, stronger cooling has been recorded in the WEP compared to the EEP (Dang, Jian, et al., 2020; Koutavas & Joanides, 2012). However, our SST compilation, together with AWI-ESM simulations, indicates that the weakest cooling occurs instead in the CEP, which rules out a monotonic zonal SST gradient over the equatorial Pacific (Figure 2; Figure S3 in Supporting Information S1). Drawing on modern analogs (Kug et al., 2009; Kug & Ham, 2011; Zhang et al., 2015), one cannot exclude that the Pacific may have been characterized by an "eastern Pacific La Nina"-like superimposed by a "central Pacific El Niño"-like mean state during the LGM. Among other PMIP4 models, only MIROC-ES2L shows a similar mixed state (Figure S8 in Supporting Information S1). AWI-ESM simulates stronger ENSO variability, as reflected by larger standard deviation of SST over the equatorial Pacific (Figure S3 in Supporting Information S1). However, this result

differs somewhat from CESM1.2, which simulates larger SST standard deviation in the EEP, but smaller in the CEP (Thirumalai et al., 2024).

4. Conclusions

Based on a proxy-model comparison, we demonstrate that the seasonal southeasterly and northeasterly winds off Sumatra are both strengthened under LGM conditions, while winds over the Celebes Sea exhibits an enhanced westerly contribution. Altogether, these changes reflect an overall "tripole" pattern of altered IPWP convection, characterized by weakened atmospheric vertical movements over the exposed Sunda and Sahul shelves and intensified movements over the EEIO and the WEP. This tripole pattern is associated with two anomalous zonal circulation cells. The western one, located over the EEIO, occurs during summer-winter, and is likely triggered by the lower sea levels. The eastern one, suited over the WEP, emerges in autumn-winter, and is probably driven by the influence of larger ice sheets. Coupled with atmospheric circulation changes, a positive IOD-like mean state likely exists in the Indian Ocean, while the Pacific is probably characterized by an "eastern Pacific La Niña"-like mean state superposed by a "central Pacific El-Niño"-like mean state. Under such configurations, both IOD and ENSO variability are suggested to be intensified.

Data Availability Statement

The NPP data can be found in Zhou (2024). The CMIP6 and PMIP4 modeling data used in this research can be accessed as follows: AWI-ESM-1-1-LR data in Danek et al. (2020) and Shi, Yang, et al. (2020), CESM2-FV2 data in Danabasoglu (2019) and Zhu, Otto-Bliesner, Brady, et al. (2022), CESM2-WACCM-FV2 data in Danabasoglu (2019) and Zhu, Otto-Bliesner, Garcia, et al. (2022), INM-CM4-8 data in Volodin et al. (2019a, 2019b), MIROC-ES2L data in Hajima et al. (2019) and Ohgaito et al. (2019), and MPI-ESM1-2-LR data in Wieners et al. (2019) and Jungclaus et al. (2019). The data of AWI-ESM-1-1-LR sensitivity experiment can be found in Shi (2023).

Acknowledgments
This study is supported by National Natural Science Foundation of China (42206060; 42206256; 41930536). Xinquan Zhou thanks Tongji University Postdoctoral Fellowship and the full-time China Scholarship Council-Université Paris-Saclay joint PhD program. Xiaoxu Shi thanks support from the Southern Marine Science and Engineering Guangdong Laboratory (Zhuhai) (Grant SML2023SP204) and the Ocean Negative Carbon Emissions (ONCE) Program. The authors acknowledge those who contributed to the PMP4, CMIP6, and sediment core collection efforts. The authors also thank the editors and reviewers.

References

Abram, N. J., Hargreaves, J. A., Wright, N. M., Thirumalai, K., Ummenhofer, C. C., & England, M. H. (2020). Palaeoclimate perspectives on the Indian Ocean Dipole. *Quaternary Science Reviews*, *237*, 106302. https://doi.org/10.1016/j.quascirev.2020.106302

Anand, P., Elderfield, H., & Conte, M. H. (2003). Calibration of Mg/Ca thermometry in planktonic foraminifera from a sediment trap time series. *Paleoceanography*, *18*(2), 1050. https://doi.org/10.1029/2002PA000846

Bassinot, F. C., Marzin, C., Braconnot, P., Marti, O., Mathien-Blard, E., Lombard, F., & Bopp, L. (2011). Holocene evolution of summer winds and marine productivity in the tropical Indian Ocean in response to insolation forcing: Data-model comparison. *Climate of the Past*, *7*(3), 815–829. https://doi.org/10.5194/cp-7-815-2011

Beaufort, L., Lancelot, Y., Camberlin, P., Cayre, O., Vincent, E., Bassinot, F., & Labeyrie, L. (1997). Insolation cycles as a major control of equatorial Indian Ocean primary production. *Science*, *278*(5342), 1451–1454. https://doi.org/10.1126/science.278.5342.1451

Behrenfeld, M. J., & Falkowski, P. G. (1997). Photosynthetic rates derived from satellite-based chlorophyll concentration. *Limnology & Oceanography*, *42*, 1–20. https://doi.org/10.4319/lo.1997.42.1.0001

Braconnot, P., Harrison, S. P., Kageyama, M., Bartlein, P. J., Masson-Delmotte, V., Abe-Ouchi, A., et al. (2012). Evaluation of climate models using palaeoclimatic data. *Nature Climate Change*, *2*(6), 417–424. https://doi.org/10.1038/nclimate1456

Brierley, C., Thirumalai, K., Grindrod, E., & Barnsley, J. (2023). Indian Ocean variability changes in the paleoclimate modelling intercomparison project. *Climate of the Past*, *19*(3), 681–701. https://doi.org/10.5194/cp-19-681-2023

Brown, J. R., Brierley, C. M., An, S.-I., Guarino, M.-V., Stevenson, S., Williams, C. J. R., et al. (2020). Comparison of past and future simulations of ENSO in CMIP5/PMIP3 and CMIP6/PMIP4 models. *Climate of the Past*, *16*(5), 1777–1805. https://doi.org/10.5194/cp-16-1777-2020

Carolin, S. A., Cobb, K. M., Adkins, J. F., Clark, B., Conroy, J. L., Lejau, S., et al. (2013). Varied response of western Pacific hydrology to climate forcings over the last glacial period. *Science*, *340*(6140), 1564–1566. https://doi.org/10.1126/science.1233797

Chang, C.-P., Wang, Z., Ju, J., & Li, T. (2004). On the relationship between western maritime continent monsoon rainfall and ENSO during northern winter. *Journal of Climate*, *17*(3), 665–672. https://doi.org/10.1175/1520-0442(2004)017<0665:OTRBWM>2.0.CO;2

Chevalier, M., Brewer, S., & Chase, B. M. (2017). Qualitative assessment of PMIP3 rainfall simulations across the eastern African monsoon domains during the mid-Holocene and the Last Glacial Maximum. *Quaternary Science Reviews*, *156*, 107–120. https://doi.org/10.1016/j.quascirev.2016.11.028

Cléroux, C., Cortijo, E., Anand, P., Labeyrie, L., Bassinot, F., Caillon, N., & Duplessy, J.-C. (2008). Mg/Ca and Sr/Ca ratios in planktonic foraminifera: Proxies for upper water column temperature reconstruction. *Paleoceanography*, *23*(3), PA3214. https://doi.org/10.1029/2007PA001505

Conway, D., Hanson, C. E., Doherty, R., & Persechino, A. (2007). GCM simulation of the Indian Ocean dipole influence on East African rainfall: Present and future. *Geophysical Research Letters*, *34*(3), L03705. https://doi.org/10.1029/2006GL027597

Currie, J. C., Lengaigne, M., Vialard, J., Kaplan, D. M., Aumont, O., Naqvi, S. W. A., & Maury, O. (2013). Indian Ocean Dipole and El Niño/southern oscillation impacts on regional chlorophyll anomalies in the Indian Ocean. *Biogeosciences*, *10*, 6677–6698. https://doi.org/10.5194/bg-10-6677-2013

Danabasoglu, G. (2019). NCAR CESM2-FV2 model output prepared for CMIP6 CMIP piControl [Dataset]. *Earth System Grid Federation*. https://doi.org/10.22033/ESGF/CMIP6.11301

19448007, 2025, 6, Downloaded from https://agupubs.onlinelibrary.wiley.com/doi/10.1029/2024GL112276 by Ifremer Centre Bretagne Blp, Wiley Online Library on [21/03/2025]. See the Terms and Conditions (https://onlinelibrary.wiley.com/terms-and-conditions) on Wiley Online Library for rules of use; OA articles are governed by the applicable Creative Commons License

Danek, C., Shi, X., Stepanek, C., Yang, H., Barbi, D., Hegewald, J., & Lohmann, G. (2020). AWI AWI-ESM1.1LR model output prepared for CMIP6 CMIP piControl [Dataset]. *Earth System Grid Federation*. https://doi.org/10.22033/ESGF/CMIP6.9335

Dang, H., Jian, Z., Wang, Y., Mohtadi, M., Rosenthal, Y., Ye, L., et al. (2020). Pacific warm pool subsurface heat sequestration modulated Walker circulation and ENSO activity during the Holocene. *Science Advances*, *6*(42), eabc0402. https://doi.org/10.1126/sciadv.abc0402

Dang, H., Jian, Z., Wu, J., Bassinot, F., Wang, T., & Kissel, C. (2018). The calcification depth and Mg/Ca thermometry of Pulleniatina obliquiloculata in the tropical Indo-Pacific: A core-top study. *Marine Micropaleontology*, *145*, 28–40. https://doi.org/10.1016/j.marmicro.2018.11.001

Dang, H., Wu, J., Xiong, Z., Qiao, P., Li, T., & Jian, Z. (2020). Orbital and sea-level changes regulate the iron-associated sediment supplies from Papua New Guinea to the equatorial Pacific. *Quaternary Science Reviews*, *239*, 106361. https://doi.org/10.1016/j.quascirev.2020.106361

De Deckker, P. (2016). The Indo-Pacific warm pool: Critical to world oceanography and world climate. *Geoscience Letters*, *3*(1), 20. https://doi.org/10.1186/s40562-016-0054-3

DiNezio, P. N., Clement, A., Vecchi, G. A., Soden, B., Broccoli, A. J., Otto-Bliesner, B. L., & Braconnot, P. (2011). The response of the Walker circulation to Last Glacial Maximum forcing: Implications for detection in proxies. *Paleoceanography*, *26*(3), PA3217. https://doi.org/10.1029/2010PA002083

DiNezio, P. N., & Tierney, J. E. (2013). The effect of sea level on glacial Indo-Pacific climate. *Nature Geoscience*, *6*, 485–491. https://doi.org/10.1038/ngeo1823

DiNezio, P. N., Tierney, J. E., Otto-Bliesner, B. L., Timmermann, A., Bhattacharya, T., Rosenbloom, N., & Brady, E. (2018). Glacials changes in tropical climate amplified by the Indian Ocean. *Science Advances*, *4*(12), eaat9658. https://doi.org/10.1126/sciadv.aat9658

Di Nezio, P. N., Timmermann, A., Tierney, J. E., Jin, F.-F., Otto-Bliesner, B., Rosenbloom, N., et al. (2016). The climate response of the Indo-Pacific warm pool to glacial sea level. *Paleoceanography*, *31*(6), 866–894. https://doi.org/10.1002/2015PA002890

Elderfield, H., & Ganssen, G. (2000). Past temperature and $\delta^{18}O$ of surface ocean waters inferred from foraminiferal Mg/Ca ratios. *Nature*, *405*(6785), 442–445. https://doi.org/10.1038/35013033

Eyring, V., Bony, S., Meehl, G. A., Senior, C. A., Stevens, B., Stouffer, R. J., & Taylor, K. E. (2016). Overview of the coupled model Intercomparison Project phase 6 (CMIP6) experimental design and organization. *Geoscientific Model Development*, *9*(5), 1937–1958. https://doi.org/10.5194/gmd-9-1937-2016

Fan, W., Jian, Z., Chu, Z., Dang, H., Wang, Y., Bassinot, F., et al. (2018). Variability of the Indonesian throughflow in the Makassar strait over the last 30 ka. *Scientific Reports*, *8*(1), 5678. https://doi.org/10.1038/s41598-018-24055-1

Hajima, T., Abe, M., Arakawa, O., Suzuki, T., Komuro, Y., Ogura, T., et al. (2019). MIROC MIROC-ES2L model output prepared for CMIP6 CMIP piControl [Dataset]. *Earth System Grid Federation*. https://doi.org/10.22033/ESGF/CMIP6.5710

Hendon, H. H. (2003). Indonesian rainfall variability: Impacts of ENSO and local air-sea interaction. *Journal of Climate*, *16*(11), 1775–1790. https://doi.org/10.1175/1520-0442(2003)016<1775:IRVIOE>2.0.CO;2

Hendrawan, I. G., Asai, K., Triwahyuni, A., & Lestari, D. V. (2019). The interannual rainfall variability in Indonesia corresponding to El Niño southern oscillation and Indian Ocean Dipole. *Acta Oceanologica Sinica*, *38*(7), 57–66. https://doi.org/10.1007/s13131-019-1457-1

Hernández-Almeida, I., Ausín, B., Saavedra-Pellitero, M., Baumann, K. H., & Stoll, H. M. (2019). Quantitative reconstruction of primary productivity in low latitudes during the last glacial maximum and the mid-to-late Holocene from a global *Florisphaera profunda* calibration dataset. *Quaternary Science Reviews*, *205*, 166–181. https://doi.org/10.1016/j.quascirev.2018.12.016

Hersbach, H., Bell, B., Berrisford, P., Hirahara, S., Horányi, A., Muñoz-Sabater, J., et al. (2020). The ERA5 global reanalysis. *Quarterly Journal of the Royal Meteorological Society*, *146*(730), 1999–2049. https://doi.org/10.1002/qj.3803

Huang, E., Yuan, Z., Wang, S., Yang, Y., Jia, G., & Tian, J. (2024). Expansion of grasslands across glacial Sundaland caused by enhanced precipitation seasonality. *Quaternary Science Reviews*, *337*, 108824. https://doi.org/10.1016/j.quascirev.2024.108824

Jungclaus, J., Mikolajewicz, U., Kapsch, M.-L., D'Agostino, R., Wieners, K.-H., Giorgetta, M., et al. (2019). MPI-M MPI-ESM1.2-LR model output prepared for CMIP6 PMIP lgm [Dataset]. *Earth System Grid Federation*. https://doi.org/10.22033/ESGF/CMIP6.6642

Kageyama, M., Albani, S., Braconnot, P., Harrison, S. P., Hopcroft, P. O., Ivanovic, R. F., et al. (2017). The PMIP4 contribution to CMIP6 – Part 4: Scientific objectives and experimental design of the PMIP4-CMIP6 Last Glacial Maximum experiments and PMIP4 sensitivity experiments. *Geoscientific Model Development*, *10*(11), 4035–4055. https://doi.org/10.5194/gmd-10-4035-2017

Kageyama, M., Braconnot, P., Harrison, S. P., Haywood, A. M., Jungclaus, J. H., Otto-Bliesner, B. L., et al. (2018). The PMIP4 contribution to CMIP6 – Part 1: Overview and over-arching analysis plan. *Geoscientific Model Development*, *11*(3), 1033–1057. https://doi.org/10.5194/gmd-11-1033-2018

Koutavas, A., & Joanides, S. (2012). El Niño-southern oscillation extreme in the Holocene and last glacial maximum. *Paleoceanography*, *27*(4), PA4208. https://doi.org/10.1029/2012PA002378

Kug, J.-S., & Ham, Y.-G. (2011). Are there two types of La Niña? *Geophysical Research Letters*, *38*(16), L16704. https://doi.org/10.1029/2011GL048237

Kug, J.-S., Jin, F.-F., & An, S.-L. (2009). Two types of El Niño events: Cold tongue El Niño and warm pool El Niño. *Journal of Climate*, *22*(6), 1499–1515. https://doi.org/10.1175/2008JCLI2624.1

Lea, D. W., Pak, D. K., & Spero, H. J. (2000). Climate impact of late Quaternary equatorial Pacific sea surface temperature variations. *Science*, *289*(5485), 1719–1724. https://doi.org/10.1126/science.289.5485.1719

Lea, C. H., Elderfield, H., & Wilson, P. A. (2000). Cenozoic deep-sea temperatures and global ice volumes from Mg/Ca in benthic foraminiferal calcite. *Science*, *287*, 269–272. https://doi.org/10.1126/science.287.5451.26

Lévy, M., Shankar, D., André, J.-M., Shenoi, S. S., Durand, F., & de Boyer Montégut, C. (2007). Basin-wide seasonal evolution of the Indian Ocean's phytoplankton blooms. *Journal of Geophysical Research*, *112*(C12), C12012. https://doi.org/10.1029/2007JC004090

Lückge, A., Mohtadi, M., Rühlemann, C., Scheeder, G., Vink, A., Reinhardt, L., & Wiedicke, M. (2009). Monsoon versus ocean circulation controls on paleoenvironmental conditions off southern Sumatra during the past 300,000 years. *Paleoceanography*, *24*(1), PA1208. https://doi.org/10.1029/2008pa001627

Marchant, R., Mumbi, C., Behera, S., & Yamagata, T. (2006). The Indian Ocean Dipole – The unsung driver of climatic variability in east Africa. *African Journal of Ecology*, *45*(1), 4–16. https://doi.org/10.1111/j.1365-2028.2006.00707.x

McCreary, J. P., Murtugudde, R., Vialard, J., Vinayachandran, P. N., Wiggert, J. D., Hood, R. R., et al. (2009). Biophysical processes in the Indian Ocean. In J. D. Wigger, R. R. Hood, S. W. A. Naqvi, K. H. Brink, & S. L. Smith (Eds.), *Indian Ocean biogeochemical processes and ecological variability* (Vol. 185, pp. 9–32). Geophysical Monograph Series. https://doi.org/10.1029/2008GM000768

Mohtadi, M., Prange, M., Schefuß, E., & Jennerjahn, T. C. (2017). Late Holocene slowdown of the Indian Ocean Walker circulation. *Nature Communications*, *8*(1), 1015. https://doi.org/10.1038/s41467-017-00855-3

Molfino, B., & McIntyre, A. (1990). Precessional forcing of nutricline dynamics in the equatorial Atlantic. *Science*, *249*(4970), 766–769. https://doi.org/10.1126/science.249.4970.766

19448007, 2025, 6, Downloaded from https://agupubs.onlinelibrary.wiley.com/doi/10.1029/2024GL112276 by Ifremer Centre Bretagne Blp, Wiley Online Library on [21/03/2025]. See the Terms and Conditions (https://onlinelibrary.wiley.com/terms-and-conditions) on Wiley Online Library for rules of use; OA articles are governed by the applicable Creative Commons License

Monteagudo, M. M., Lynch-Stieglitz, J., Marchitto, T. M., & Schmidt, M. W. (2021). Central equatorial Pacific cooling during the last glacial maximum. *Geophysical Research Letters*, *48*(3), e2020GL088592. https://doi.org/10.1029/2020GL088592

Niedermeyer, E. V., Sessions, A. L., Feakins, S., & Mohtadi, M. (2014). Hydroclimate of the western Indo-Pacific warm pool during the past 24,000 years. *Proceedings of the National Academy of Sciences*, *111*(26), 9402–9406. https://doi.org/10.1073/pnas.1323585111

Ohgaito, R., Abe-Ouchi, A., Abe, M., Arakawa, O., Ogochi, K., Hajima, T., et al. (2019). MIROC MIROC-ES2L model output prepared for CMIP6 PMIP lgm. Version YYYYMMDD[1]. *Earth System Grid Federation*. https://doi.org/10.22033/ESGF/CMIP6.5644

Partin, J., Cobb, K., Adkins, J., Clark, B., & Fernandez, D. P. (2007). Millennial-scale trends in west Pacific warm pool hydrology since the Last Glacial Maximum. *Nature*, *449*(7161), 452–455. https://doi.org/10.1038/nature06164

Patterson, R. T., & Fishbein, E. (1989). Re-examination of the statistical methods used to determine the number of point counts needed for micropaleontological quantitative research. *Journal of Paleontology*, *63*(2), 245–248. https://doi.org/10.1017/s0022336000019272

Ropelewski, C. F., & Halpert, M. S. (1986). Northern American precipitation and temperature patterns associated with the El Niño/Southern Oscillation (ENSO). *Monthly Weather Review*, *114*(12), 2352–2362. https://doi.org/10.1175/1520-0493(1986)114<2352:NAPATP>2.0.CO;2

Ruan, Y., Mohtadi, M., van der Kaars, S., Dupont, L. M., Hebbeln, D., & Schefuß, E. (2019). Differential hydro-climatic evolution of East Javanese ecosystems over the past 22,000 years. *Quaternary Science Reviews*, *218*, 49–60. https://doi.org/10.1016/j.quascirev.2019.06.015

Ryan, W. B. F., Carbotte, S. M., Coplan, J. O., O'Hara, S., Melkonian, A., Arko, R., et al. (2009). Global multi-resolution topography synthesis. *Geochemistry, Geophysics, Geosystems*, *10*(3), Q03014. https://doi.org/10.1029/2008GC002332

Saji, N. H., Goswami, B. N., Vinayachandran, P. N., & Yamagata, T. (1999). A dipole mode in the tropical Indian Ocean. *Nature*, *401*(6751), 360–363. https://doi.org/10.1038/43854

Saji, N. H., & Yamagata, T. (2003). Possible impacts of Indian Ocean Dipole mode events on global climate. *Climate Research*, *25*, 151–169. https://doi.org/10.3354/cr025151

Shi, X. (2023). LGM simulations based on AWIESM [Dataset]. *Zenodo*. https://doi.org/10.5281/zenodo.8063488

Shi, X., Lohmann, G., Sidorenko, D., & Yang, H. (2020). Early-Holocene simulations using different forcings and resolutions in AWI-ESM. *The Holocene*, *30*(7), 996–1015. https://doi.org/10.1177/0959683620908634

Shi, X., Werner, M., Yang, H., D'Agostino, R., Liu, J., Yang, C., & Lohmann, G. (2023). Unraveling the complexities of the last glacial maximum climate: The role of individual boundary conditions and forcings. *Climate of the Past*, *19*(11), 2157–2175. https://doi.org/10.5194/cp-19-2157-2023

Shi, X., Yang, H., Danek, C., & Lohmann, G. (2020). AWI AWI-ESM1.1LR model output prepared for CMIP6 PMIP lgm [Dataset]. *Earth System Grid Federation*. https://doi.org/10.22033/ESGF/CMIP6.9330

Sidorenko, D., Rackow, T., Jung, T., Semmler, T., Barbi, D., Danilov, S., et al. (2015). Towards multi-resolution global climate modeling with ECHAM6–FESOM. Part I: Model formulation and mean climate. *Climate Dynamics*, *44*(3–4), 757–780. https://doi.org/10.1007/s00382-014-2290-6

Supari, Tang, F., Salimun, E., Aldrian, E., Sopaheluwakan, A., & Juneng, L. (2018). ENSO modulation of seasonal rainfall and extremes in Indonesia. *Climate Dynamics*, *51*, 2259–2580. https://doi.org/10.1007/s00382-017-4028-8

Tedeschi, R. G., Cavalcanti, I. F. A., & Grimm, A. M. (2013). Influences of two types of ENSO on South American precipitation. *International Journal of Climatology*, *33*(6), 1382–1400. https://doi.org/10.1002/joc.3519

Thirumalai, K., DiNezio, P. N., Partin, J. W., Liu, D., Coasta, K., & Jacobel, A. (2024). Future increase in extreme El Niño supported by past glacial changes. *Nature*, *634*(8033), 374–380. https://doi.org/10.1038/s41586-024-07984-y

Thirumalai, K., DiNezio, P. N., Tierney, J. E., Puy, M., & Mohtadi, M. (2019). An El Niño mode in the glacial Indian ocean? *Paleoceanography and Paleoclimatology*, *34*(8), 1316–1327. https://doi.org/10.1029/2019PA003669

Tian, Z., & Juang, D. (2019). Weakening and eastward shift of the tropical Pacific walker circulation during the last glacial maximum. *Boreas*, *49*(1), 200–210. https://doi.org/10.1111/bor.12417

Volodin, E., Mortikov, E., Gritsun, A., Lykossov, V., Galin, V., Diansky, N., et al. (2019a). INM INM-CM4-8 model output prepared for CMIP6 CMIP piControl [Dataset]. *Earth System Grid Federation*. https://doi.org/10.22033/ESGF/CMIP6.5080

Volodin, E., Mortikov, E., Gritsun, A., Lykossov, V., Galin, V., Diansky, N., et al. (2019b). INM INM-CM4-8 model output prepared for CMIP6 PMIP lgm [Dataset]. *Earth System Grid Federation*. https://doi.org/10.22033/ESGF/CMIP6.5075

Wieners, K.-H., Giorgetta, M., Jungclaus, J., Reick, C., Esch, M., Bittner, M., et al. (2019). MPI-M MPI-ESM1.2-LR model output prepared for CMIP6 CMIP piControl [Dataset]. *Earth System Grid Federation*. https://doi.org/10.22033/ESGF/CMIP6.6675

Wiggert, J. D., Vialard, J., & Behrenfeld, M. J. (2009). Basin-wide modification of dynamical and biogeochemical processes by the positive phase of the Indian Ocean Dipole during the SeaWiFS era. In J. D. Wigger, R. R. Hood, S. W. A. Naqvi, K. H. Brink, & S. L. Smith (Eds.), *Indian Ocean biogeochemical processes and ecological variability* (Vol. 185, pp. 9–32). Geophysical Monograph Series. https://doi.org/10.1029/2008GM000776

Wu, J., Liu, Z., & Zhou, C. (2013). Provenance and supply of Fe-enriched terrigenous sediments in the western equatorial Pacific and their relation to precipitation variations during the late Quaternary. *Global and Planetary Change*, *108*, 56–71. https://doi.org/10.1016/j.gloplacha.2013.06.002

Wurtzel, J. B., Abram, N. J., Lewis, S. C., Bajo, P., Hellstrom, J. C., Troitzsch, U., & Heslop, D. (2018). Tropical Indo-Pacific hydroclimate response to North Atlantic forcing during the last deglaciation as recorded by a speleothem from Sumatra, Indonesia. *Earth and Planetary Science Letters*, *492*, 264–278. https://doi.org/10.1016/j.epsl.2018.04.001

Yin, Z., Dong, Q., Kong, F., Cao, D., & Long, S. (2020). Seasonal and interannual variability of the Indo-Pacific Warm Pool and its associated climate factors based on remote sensing. *Remote Sensing*, *12*(7), 1062. https://doi.org/10.3390/rs12071062

Yu, Z., Tang, X., Colin, C., Wilson, D. J., Zhou, X., Song, L., et al. (2023). Millennial-scale precipitation variability in the Indo-Pacific region over the last 40 Kyr. *Geophysical Research Letters*, *50*(2), e2022GL101646. https://doi.org/10.1029/2022GL101646

Zhang, W., Wang, Y., Jin, F.-F., Stuecker, M. F., & Turner, A. G. (2015). Impact of different El Niño types on the El Niño/IOD relation-ship. *Geophysical Research Letters*, *42*(20), 8570–8576. https://doi.org/10.1002/2015GL065703

Zhang, Y., Xu, J., Li, G., Lu, Z., Jiang, Z., Zhang, W., & Liu, Y. (2023). ENSO-like evolution of the tropical Pacific climate mean state and its potential causes since 300ka. *Quaternary Science Reviews*, *315*, 108241. https://doi.org/10.1016/j.quascirev.2023.108241

Zhou, X. (2024). Reconstructed net primary productivity of marine sediment cores MD98-2152, BAR94-24, MD85-666, and MD98-2178 [Dataset]. *Zenodo*. https://doi.org/10.5281/zenodo.13486390

Zhou, X., Duchamp-Alphonse, S., Bassinot, F., & Liu, C. (2024). Summer and autumn insolation as the pacemaker of surface wind and precipitation dynamics over tropical Indian Ocean during the Holocene: Insights from paleoproductivity records and paleoclimate simulations. *Paleoceanography and Paleoclimatology*, *39*(1), e2023PA004786. https://doi.org/10.1029/2023PA004786

Zhou, X., Jin, X., Shi, X., & Liu, C. (2023). The change in convection over the Indo-Pacific warm pool in the mid-Holocene and its influence on South Asian precipitation. *Quaternary Science Reviews*, *322*, 108399. https://doi.org/10.1016/j.quascirev.2023.108399

19448007, 2025, 6, Downloaded from https://agupubs.onlinelibrary.wiley.com/doi/10.1029/2024GL112276 by Ifremer Centre Bretagne Blp, Wiley Online Library on [21/03/2025]. See the Terms and Conditions (https://onlinelibrary.wiley.com/terms-and-conditions) on Wiley Online Library for rules of use; OA articles are governed by the applicable Creative Commons License

Zhu, J., Otto-Bliesner, B. L., Brady, E. C., Gettelman, A., Bacmeister, J. T., Neale, R. B., et al. (2022). LGM paleoclimate constraints inform cloud parameterizations and equilibrium climate sensitivity in CESM2. *Journal of Advances in Modeling Earth Systems*, *14*(4), e2021MS002776. https://doi.org/10.1029/2021MS002776

Zhu, J., Otto-Bliesner, B. L., Garcia, R., Brady, E. C., Mills, M., Kinnison, D., & Lamarque, J.-F. (2022b). Small impact of stratospheric dynamics and chemistry on the surface temperature of the Last Glacial Maximum in CESM2(WACCM6ma). *Geophysical Research Letters*, *49*(20), e2022GL099875. https://doi.org/10.1029/2022GL099875

References From the Supporting Information

Beaufort, L., Barbarin, N., & Gally, Y. (2014). Optical measurements to determine the thickness of calcite crystals and the mass of thin carbonate particles such as coccoliths. *Nature Protocols*, *9*(3), 633–642. https://doi.org/10.1038/nprot.2014.028

Bordiga, M., Bartol, M., & Henderiks, J. (2015). Absolute nannofossil abundance estimates: Quantifying the pros and cons of different techniques. *Revue de micropaéontologie*, *58*(3), 155–165. https://doi.org/10.1016/j.revmic.2015.05.002

Benway, H. M., Mix, A. C., Haley, B. A., & Klinkhammer, G. P. (2006). Eastern Pacific warm pool paleosalinity and climate variability: 0-30 kyr. *Paleoceanography*, *21*(3), PA3008. https://doi.org/10.1029/2005PA001208

Duchamp-Alphonse, S., Siani, G., Michel, E., Beaufort, L., Gally, Y., & Jaccard, S. L. (2018). Enhanced ocean-atmosphere carbon partitioning via the carbonate counter pump during the last deglacial. *Nature Communications*, *9*(1), 2396. https://doi.org/10.1038/s41467-018-04625-7

Fan, W., Jian, Z., Bassinot, F., & Chu, Z. (2013). Holocene centennial-scale changes of the Indonesian and south China sea throughflows: Evidences from the Makassar strait. *Global and Planetary Change*, *111*, 111–117. https://doi.org/10.1016/j.gloplacha.2013.08.017

Hajima, T., Watanabe, M., Yamamoto, A., Tatebe, H., Noguchi, M. A., Abe, M., et al. (2020). Development of the MIROC-ES2L Earth system model and the evaluation of biogeochemical processes and feedbacks. *Geoscientific Model Development*, *13*, 2197–2244. https://doi.org/10.5194/gmd-13-2197-2020

Jian, Z., Wang, Y., Dang, H., Lea, D. W., Liu, Z., Jin, H., & Yin, Y. (2020). Half-precessional cycle of thermocline temperature in the western equatorial Pacific and its bihemispheric dynamics. *Proceedings of the National Academy of Sciences*, *117*(13), 7044–7051. https://doi.org/10.1073/pnas.1915510117

Koné, V., Aumont, O., Lévy, M., & Resplandy, L. (2009). Physical and biogeochemical controls of the phytoplankton seasonal cycle in the Indian Ocean: A model study. In J. D. Wigger, R. R. Hood, S. W. A. Naqvi, K. H. Brink, & S. L. Smith (Eds.), *Indian Ocean biogeochemical processes and ecological variability* (Vol. 185, pp. 9–32). Geophysical Monograph Series. https://doi.org/10.1029/2008GM000700

Kripalani, R. H., & Kumar, P. (2004). Northeast monsoon rainfall variability over south peninsular India vis-à-vis the Indian Ocean dipole mode. *International Journal of Climatology*, *24*(10), 1267–1282. https://doi.org/10.1002/joc.1071

Lea, D. W., Pak, D. K., Belanger, C. L., Spero, H. J., Hall, M. A., & Shackleton, N. J. (2006). Paleoclimate history of Galápagos surface waters over the last 135,000 yr. *Quaternary Science Reviews*, *25*(11–12), 1152–1167. https://doi.org/10.1016/j.quascirev.2005.11.010

Lupi, C., Bordiga, M., Sacchi, R., Galinetto, P., Beaufort, L., & Cobianchi, M. (2016). Do sample preparation techniques affect the relative abundance of *Florisphaera profunda*? *Marine Micropaleontology*, *127*, 42–49. https://doi.org/10.1016/j.marmicro.2016.07.007

Mauritsen, T., Bader, J., Becker, T., Behrens, J., Bittner, M., Brokopf, R., et al. (2019). Developments in the MPI-M earth system model version 1.2 (MPI-ESM1.2) and its response to increasing CO_2. *Journal of Advances in Modeling Earth Systems*, *11*(4), 998–1038. https://doi.org/10.1029/2018MS001400

Mohtadi, M., Steinke, S., Groeneveld, J., Fink, H. G., Rixen, T., Hebbeln, D., et al. (2009). Low-latitude control on seasonal and interannual changes in planktonic foraminiferal flux and shell geochemistry off south Java: A sediment trap study. *Paleoceanography*, *24*(1), PA1201. https://doi.org/10.1029/2008PA001636

Mohtadi, M., Steinke, S., Lückge, A., Groeneveld, J., & Hathorne, E. D. (2010). Glacial to Holocene surface hydrography of the tropical eastern Indian Ocean. *Earth and Planetary Science Letters*, *292*(1–2), 89–97. https://doi.org/10.1016/j.epsl.2010.01.024

Mohtadi, M., Prange, M., Oppo, D. W., De Pol-Holz, R., Merkel, U., Zhang, X., et al. (2014). North Atlantic forcing of tropical Indian Ocean climate. *Nature*, *509*(7498), 76–80. https://doi.org/10.1038/nature13196

Mohtadi, M., Oppo, D. W., Lückge, A., De Pol-Holz, R., Steinke, S., Groeneveld, J., et al. (2011). Reconstructing the thermal structure of the upper ocean: Insights from planktic foraminifera shell chemistry and alkenones in modern sediments of the tropical eastern Indian Ocean. *Paleoceanography*, *26*(3), PA3219. https://doi.org/10.1029/2011PA002132

Nayagam, L. R., Janardanan, R., & Mohan, H. S. R. (2009). Variability and teleconnectivity of the northeast monsoon rainfall over India. *Global and Planetary Change*, *69*, 225–231. https://doi.org/10.1016/j.gloplacha.2009.10.005

Pena, L. D., Cacho, I., Ferretti, P., & Hall, M. A. (2008). El Niño–Southern Oscillation–like variability during glacial terminations and interlatitudinal teleconnections. *Paleoceanography*, *23*(3), PA3101. https://doi.org/10.1029/2008PA001620

Prasanna, V., & Yasunari, T. (2008). Interannual variability of atmospheric water balance over South Peninsular India and Sri Lanka during the northeast monsoon season. *International Journal of Climatology*, *28*(15), 1997–2009. https://doi.org/10.1002/joc.1683

Romahn, S., Mackensen, A., Groeneveld, J., & Pätzold, J. (2014). Deglacial intermediate water reorganization: New evidence from the Indian Ocean. *Climate of the Past*, *10*(1), 293–303. https://doi.org/10.5194/cp-10-293-2014

Rippert, N., Baumann, K.-H., & Pätzold, J. (2015). Thermocline fluctuations in the western tropical Indian Ocean during the past 35 ka. *Journal of Quaternary Science*, *30*(3), 201–210. https://doi.org/10.1002/jqs.2767

Sadekov, A. Y., Ganeshram, R., Pichevin, L., Berdin, R., McClymont, E., Elderfield, H., & Tudhope, A. W. (2013). Palaeoclimate reconstructions reveal a strong link between El Niño-Southern Oscillation and Tropical Pacific mean state. *Nature Communications*, *4*(1), 2692. https://doi.org/10.1038/ncomms3692

Susanto, R. D., Gordon, A. L., & Zheng, Q. (2001). Upwelling along the coasts of Java and Sumatra and its relation to ENSO. *Geophysical Research Letters*, *28*(8), 1599–1602. https://doi.org/10.1029/2000GL011844

Southon, J., Kashgarian, M., Fontugne, M., Metivier, B., & Yim, W. W.-S. (2002). Marine reservoir corrections for the Indian Ocean and southeast Asia. *Radiocarbon*, *44*(1), 167–180. https://doi.org/10.1017/S0033822200064778

Schröder, J. F., Holbourn, A., Kuhnt, W., & Küssner, K. (2016). Variations in sea surface hydrology in the southern Makassar Strait over the past 26 kyr. *Quaternary Science Reviews*, *154*, 143–156. https://doi.org/10.1016/j.quascirev.2016.10.018

Schröder, J. F., Kuhnt, W., Holbourn, A., Beil, S., Zhang, P., Hendrizan, M., & Xu, J. (2018). Deglacial warming and hydroclimate variability in the central Indonesian archipelago. *Paleoceanography and Paleoclimatology*, *33*(9), 974–993. https://doi.org/10.1029/2018PA003323

Stott, L., Poulsen, C., Lund, S., & Thunell, R. (2002). Super ENSO and global climate oscillations at millennial time scales. *Science*, *297*(5579), 222–226. https://doi.org/10.1126/science.1071627

19448007, 2025, 6, Downloaded from https://agupubs.onlinelibrary.wiley.com/doi/10.1029/2024GL112276 by Ifremer Centre Bretagne Blp, Wiley Online Library on [21/03/2025]. See the Terms and Conditions (https://onlinelibrary.wiley.com/terms-and-conditions) on Wiley Online Library for rules of use; OA articles are governed by the applicable Creative Commons License

Stott, L., Timmermann, A., & Thunell, R. (2007). Southern Hemisphere and deep-sea warming led deglacial atmospheric CO_2 rise and tropical warming. *Science*, *318*(5849), 435–438. https://doi.org/10.1126/science.1143791

Singh, N., & Sontakke, N. A. (1999). On the variability and prediction of rainfall in the post-monsoon season over India. *International Journal of Climatology*, *19*(3), 309–339. https://doi.org/10.1002/(SICI)1097-0088(19990315)19:3<309::AID-JOC361>3.0.CO;2-%23

Tan, C. K., Ishizaka, J., Matsumura, S., Yusoff, F. M., & Mohamed, M. I. H. (2006). Seasonal variability of SeaWiFS chlorophyll a in the Malacca straits in relation to Asian monsoon. *Continental Shelf Research*, *26*(2), 168–178. https://doi.org/10.1016/j.csr.2005.09.008

Volodin, E. M., Mortikov, E. V., Kostrykin, S. V., Galin, V. Y., Lykossov, V. N., Gritsun, A. S., et al. (2018). Simulation of the modern climate using the INM-CM48 climate model. *Russian Journal of Numerical Analysis and Mathematical Modelling*, *33*(6), 367–374. https://doi.org/10.1515/rnam-2018-0032

Visser, K., Thunell, R., & Stott, L. (2003). Magnitude and timing of temperature change in the Indo-Pacific warm pool during deglaciation. *Nature*, *421*(6919), 152–155. https://doi.org/10.1038/nature01297

Wang, X., Jian, Z., Lückge, A., Wang, Y., Dang, H., & Mohtaid, M. (2018). Precession-paced thermocline water temperature changes in response to upwelling conditions off southern Sumatra over the past 300,000 years. *Quaternary Science Reviews*, *192*, 123–134. https://doi.org/10.1016/j.quascirev.2018.05.035

Wiggert, J. D., Murtugudde, R. G., & Christian, J. R. (2006). Annual ecosystem variability in the tropical Indian Ocean: Results of a coupled bio-physical ocean general circulation model. *Deep-Sea Research II*, *53*(5–7), 644–676. https://doi.org/10.1016/j.dsr2.2006.01.027

Zhou, X., Lyu, X., Liu, C., Liu, Z., Li, Q., Jin, X., et al. (2019). Depositional mechanisms for upper Miocene sediments in the South China Sea central basin: Evidence from calcareous nannofossils. *Marine Micropaleontology*, *151*, 101768. https://doi.org/10.1016/j.marmicro.2019.101768

19448007, 2025, 6, Downloaded from https://agupubs.onlinelibrary.wiley.com/doi/10.1029/2024GL112276 by Ifremer Centre Bretagne Blp, Wiley Online Library on [21/03/2025]. See the Terms and Conditions (https://onlinelibrary.wiley.com/terms-and-conditions) on Wiley Online Library for rules of use; OA articles are governed by the applicable Creative Commons License